HHS Public Access

Author manuscript

Langmuir. Author manuscript; available in PMC 2019 December 11.

Published in final edited form as:

Langmuir. 2018 December 11; 34(49): 15084–15092. doi:10.1021/acs.langmuir.8b02271.

Dynamic Interactions Between Lipid Tethered DNA and Phospholipid Membranes

Patrick M. Arnott[a], **Himanshu Joshi**[#b], **Aleksei Aksimentiev**[#b], and **Stefan Howorka**[a]

[a] Department of Chemistry, Institute of Structural and Molecular Biology, University College London, London, United Kingdom

[b] Department of Physics, and Beckman Institute for Advanced Science and Technology, University of Illinois at Urbana—Champaign, Urbana, Illinois 61801, United States

[#] These authors contributed equally to this work.

Abstract

Lipid-anchored DNA can attach functional cargo to bilayer membranes in DNA nanotechnology, synthetic biology, and cell biology research. To optimize DNA anchoring, an understanding of DNA-membrane interaction in terms of binding strength, extent, and structural dynamics is required. Here we use experiments and molecular dynamics (MD) simulations to determine how membrane binding of cholesterol-modified DNA depends on electrostatic and steric factors involving lipid head-group charge, duplexed or single stranded DNA, and buffer composition. The experiments distinguish between free and membrane vesicle-bound DNA, and thereby reveal the surface density of anchored DNA and its binding affinity, something which had previously not been known. The K_d values range from 8.5 ± 4.9 to 466 ± 134 uM whereby negatively charged head-groups led to weak binding due to the electrostatic repulsion to the negatively charged DNA. Atomistic molecular dynamics simulations explain the findings and elucidate the dynamic nature of anchored DNA such as the mushroom-like conformation of single stranded DNA hovering over the bilayer surface in contrast to a straight-up conformation of double stranded DNA. The biophysical insight into binding strength to membranes as well as the molecular accessibility of DNA for hybridization to molecular cargo is expected to facilitate creating biomimetic DNA versions of natural membrane nanopores and cytoskeletons for research and nanobiotechnology.

Graphical Abstract

Corresponding Author: s.howorka@ucl.ac.uk, aksiment@illinois.edu.

Author Contributions

The manuscript was written through contributions of all authors. All authors have given approval to the final version of the manuscript.

ASSOCIATED CONTENT

Supporting Information

Molecular graphics images illustrating the conformations of dsDNA and ssDNA molecules observed in MD simulations (Figure S1); graphs detailing the effect of ion type of screening the charge of a PE/PG membrane (Figure S2); additional molecular graphics images illustrating representative conformations of tethered DNA (figure S3); graphs illustrating dependence of the following quantities on simulation time: the average tilt of the DNA molecules (Figure S4), the fraction of DNA in contact with the membrane (Figure S5), the distance between cholesterol and membrane (Figure S6), the distance between membrane and DNA (Figure S7), the distance between cholesterol and membrane (Figure S8), and the mean squared displacement of the cholesterol anchor (Figure S9); animations (Movies 1–6) illustrating MD trajectories.

The Supporting Information is available free of charge on the ACS Publications website.

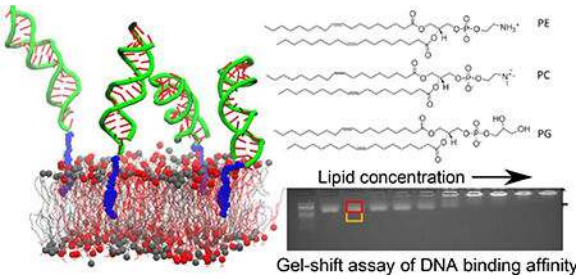

INTRODUCTION

A terminally attached lipid can anchor a DNA strand to bilayer membranes. The simple approach has impacted a range of research fields.[1] In biophysics, terminally anchored DNA permits the study of DNA hybridization in two-dimensional space compared to conventional hybridization in solution[2–5] and also allow facile visualization of membrane regions.[6] In nanobiotechnology, lipid-linked DNA enable the hybridization-mediated attachment of functional cargo[7–8] at the fluid-lipid interface to mimic the function of proteins. For example, DNA-based artificial cytoskeletons can be used to shape membrane vesicles.[9–12] Similarly, DNA-based pores can be anchored to puncture the membrane[13–18] for applications such as bio-sensing[19–21] or controlled drug release.[17] Membrane-anchored DNA nanostructures can also probe membrane interaction forces[22] or alter the composition of a lipid bilayer membrane.[23] Finally, in synthetic biology, membrane-anchored DNA can link via duplex formation vesicles to planar membranes[24] vesicles,[2, 25–26] or cells[27] often by assuming the function of membrane fusion proteins.[28–33]

Understanding the interaction of anchored DNA with bilayer membranes is important for basic science and attaining the desired performance in applications. For example, end-point-tethered DNA should be stably anchored to the membrane with high affinity. Furthermore, the DNA should be sterically accessible to enable hybridization with an incoming complementary DNA strand. This means that the DNA should neither cluster with each other nor adhere with its bases or backbone to the membrane. To understand DNA-membrane interactions, one study looked at changes in hydrodynamic radii of DNA and the effect of multiple lipid anchors.[3] Yet, there are several unanswered questions. For example, what is the affinity and surface density of end-point-tethered DNA strands, and how do both depend on experimental parameters that influence electrostatic and sterics? Charge-relevant parameters are the ionic head group of phospholipids, and the salt composition of the buffer. DNA length, the single- and double-stranded form involve both electrostatics and sterics. Further questions relate to the dynamics and molecular visualization of terminally tethered DNA. For example, under which conditions does the remaining part of the DNA strand adhere the lipid bilayer? Answering the questions would lead to a better understanding of how DNA and membranes interact and thereby form a rational basis to design targeted anchoring of DNA nanostructures or achieving defined contact between bilayers.

In this study, we use experiments and computation to examine how DNA strands with a single terminally tethered lipid anchor to and interact with synthetic lipid bilayer membranes (Figure 1A). The DNA oligonucleotides carry a cholesterol anchor tethered via a flexible

tetra(ethylene glycol)(TEG) linker at the strands' 5′ terminus (Figure 1B). To probe length and sterics, both 20 and 40 nt long oligonucleotides as well as double stranded DNA (dsDNA) and single-stranded DNA (ssDNA) are examined. The synthetic membranes are small unilamellar vesicles (SUVs) of tunable lipid composition. The lipids were chosen based on their wide use in research and to cover a representative lipid head-groups ranging from negatively charged to zwitterionic with either a tertiary or quaternary amine. The vesicles were composed of a 7:3 (ref. [17]) mixture of two phospholipids with the zwitterionic head groups: 1,2-dioleoyl-*sn*-glycero-3-phosphoethanolamine (DOPE, PE) and 1,2-dioleoyl-*sn*-glycero-3-phosphocholine (DOPC, PC) (Figure 1C). Alternatively, the membranes are a mixture of 4:1 PE and negatively charged 1,2-dioleoyl-*sn*-glycero-3-phospho-*rac*-(1′-glycerol) (DOPG, PG) (Figure 1C). In addition, the influence of two buffers is examined to probe the influence of salt composition and ionic strength. Phosphate buffered saline (PBS) contains mostly Na^+ (10 mM PO_4^{3-}, 137 mM NaCl, 2.7 mM KCl) and has an ionic strength of 0.179 M and pH = 7.4. As comparison, K^+ containing, buffer 0.3 M KCl, 15 mM Tris pH 8.0 with an ionic strength of 0.315 M was also tested. The two buffering components (PO_4^{3-} vs. amine- and alcohol containing Tris) are different, yet their concentration is considerably lower than the alkali salt components which dominate the ionic character of the solutions. Furthermore, the pH of the buffers is similar and maintains the ionization of the lipid head-groups shown in Fig. 1C.

Exploiting this wide chemical parameter space, the anchoring of cholesterol DNA to the SUVs is analyzed with gel electrophoresis to distinguish free and SUV-bound DNA and thereby infer the surface density of DNA on the membranes, as well as the affinity of the interaction. Mirroring the system explored by experiment, we construct all-atom models of arrays of dsDNA or ssDNA molecules embedded in lipid bilayer membranes[34–36] via covalently attached cholesterol anchors. The systems are solvated with explicit electrolyte (ions and water), allowing for accurate account of electrostatic interactions. The structures are animated using the molecular dynamics (MD) method that characterizes equilibrium and kinetic properties of lipid-tethered DNA systems.

The quantitative analysis shows that cholesterol-DNA can pack tightly on membranes with a maximum density of one strand per 0.02 to 0.04 nm^2, depending on the lipid composition. By comparison, affinity varies up to 50-fold depending on lipid head-group, DNA length, and buffer. Both data sets underscore the strong influence of electrostatics on the interaction of DNA and the lipid membrane. As example, negatively charged lipids lead to weakened affinity while single stranded DNA is generally undergoing close contact with zwitterionic lipids. The simulations support the data and visualize the conformations of anchored DNA molecules on membranes. The detailed understanding can improve the designs of membrane-interacting DNA nanostructures such as by tuning the membrane affinity of DNA strands, or by choosing conditions to enhance the molecular accessibility of DNA for hybridization to functional molecular cargo.

RESULTS

Analyzing the interaction of lipidated DNA and membrane vesicles with a gel shift assay.

The binding of cholesterol-modified DNA strands to small unilamellar vesicles (SUVs) was assayed with agarose gel electrophoresis. DNA strands that bound to the vesicles were separated from free DNA strands based on the size-exclusion effect of the gel. The gel matrix is wide enough to permit the electrophoretic migration of unbound DNA oligonucleotides. However, 70 to 110 nm-sized SUVs are too large for the matrix pores.

The principle of separating free from membrane-bound DNA helped determine the extent of membrane binding. In the titration experiments, the amount of vesicles, equivalent to the total surface area of membranes, was increased while the DNA concentration was held constant. The advantage of this method is that a constant DNA concentration greatly facilitates the gel electrophoretic analysis of membrane-bound vs free DNA. The alternative method of keeping the membrane surface area constant would have led to greatly varying amounts of DNA that are difficult to analyze in gels with an inherent limited linear range.

A typical read-out of a titration experiment is shown in Figure 2A for 20 nt-long ssDNA and PE/PC vesicles in PBS buffer. At low SUV / lipid concentrations, most of the cholesterol-DNA was in the unbound form and migrated into the gel. Increasing SUV concentration led to more DNA binding and a higher proportion of DNA in the SUV band at the top of the gel (Figure 2A). No free DNA was present at the highest lipid concentration. The binding of DNA is mediated by cholesterol but not electrostatic interactions as DNA without lipid-anchor did not migrate at the SUV band (not shown).

The gel shift assay revealed strong changes in the extent of membrane-binding of the cholesterol-DNA. For example, changing the lipid head groups from PE/PC (neutral) to PE/PG (negative) and replacing PBS with 0.3 M KCl resulted in an almost complete lack of binding; most DNA migrated into the gel even at the highest lipid concentration (Figure 2B). In contrast to very weak binding, the gel assay also established strong interaction. As shown in Figure 2C, the same PE/PG vesicles but dsDNA and PBS led to stronger binding than in the previous cases. Under these conditions, the critical lipid concentration at which half of the DNA is fully incorporated into the SUV shifted to left (compare Figure 2B and 2C). Hence, the gel shift assay extracts information about the extent of cholesterol-mediated anchoring as a function of membrane lipid head group, buffer, and DNA type.

Quantifying DNA Membrane Binding.

The titration results were analyzed to obtain two quantitative measures for the DNA-bilayer interaction: the affinity, and the maximum surface density of anchored DNA. Therefore, gel images were subjected to ImageJ analysis. Band intensities for free DNA, I_{DNA}, were determined within a region of interest (ROI) around the band (Figure 2A, red box) and then subtracting the background intensity of the gel $I_{\mathrm{background}}$ (Figure 2A, orange box). The data on 1- (I_{DNA} - $I_{\mathrm{background}}$) were then plotted against the lipid concentration and fitted to a Langmuir isotherm (Figure 3). The affinity of the interaction, K_d was inferred from the fits under the assumption that the varying area of membrane surface does not influence the energetics for the membrane-anchoring of DNA.

The maximum surface density was derived in a two-step process by first dividing the amount of added DNA to the total membrane surface area using equation $\delta = DNA_{max}/(0.5\ A_l\ n_l\ T_s)$ where DNA_{max} is the maximum amount of DNA loaded onto the vesicles, n_l the number of lipids per vesicle, T_s the number of SUVs, and A_l the area occupied by a single lipid molecule depending on the lipid type[37–40]. The factor 0.5 accounts for the double-leaflet structure of the bilayers. The values of δ were 0.03 molecules nm^{-2} for PE/PC and 0.04 molecules nm^{-2} for PE/PG vesicles.[3, 41] In a second step, the maximum surface density was obtained by multiplying δ with the Langmuir fit-derived value of relative binding i.e. 1-(I_{DNA} - $I_{background}$), under the assumption that 100% is equal to δ (Figure 3).

K_d and surface density were determined for DNA of both length (20 vs 40 nt), single and double stranded DNA (ss and ds), for charge neutral PE/PC membranes and predominately negatively polarized PE/PG membranes, and for low ionic strength (PBS) and high ionic strength buffer (0.3 M KCl). For each of these conditions, data were acquired in at least three independent experiments. The results of the quantitative analysis are shown in Figure 4.

The maximum surface density ranged from 0.029 ± 0.001 to 0.047 ± 0.005 molecules nm^{-2} for all conditions tested with the majority around 0.03 molecules nm^{-2} (Supporting Information, Figure S1 and Table S1). There is no clear systematic trend of how surface density depended on a single set of lipid head-group, buffer, or DNA length.

The Affinity of Lipid-Anchored DNA for Membranes is Lower for Negatively Charged Lipids but also Depends on the Buffer Composition.

In contrast to the modestly variable surface densities, the K_d for the membrane-binding of cholesterol-DNA changed up to 50-fold (Figure 4A and 4B, Supporting Information Table S1). A strong influencing factor was the membranes' lipid head-group. Each of the four DNA types bound with higher affinity (low K_d) to PE/PC than to PE/PG membranes (Figure 4A and 4B, respectively; red bars; note different y-axis) in 0.3 M KCl buffer. The lower affinity is due to electrostatic repulsion between the negatively charged lipid head groups and the phosphate groups in the backbone, as confirmed by simulations (see below).

Buffer composition also influenced the affinity. The binding on negative PE/PG membranes was weaker in 0.3 M KCl than in PBS (Figure 4A and 4B, respectively; yellow bars) when the four DNA types are compared side-by-side. The lower affinity in 0.3 M KCl is surprising because the buffer's higher ionic strength could have been expected to electrostatically screen DNA's phosphates more effectively than PBS and thereby reduce electrostatic repulsion and increase affinity. As the experimental affinity is higher in PBS, it is more probable that the different ionic composition (Na^+ vs K^+) of the buffers is the molecular reason.

Ion exchange experiments[42] and all-atom MD simulations[43] have shown that Na^+ and K^+ ions have, overall, similar affinity to dsDNA molecules, but bind to different parts of the molecule: minor (Na^+) and major (K^+) groves of the DNA.[43–44] At the same time, previous MD simulation have found Na^+ ions to interact stronger with the zwitterionic head groups of PE and PC lipid bilayers[45–46] and reduce the average area per lipid head group. Our own

MD simulations (Figure S2) also found Na^+ ions to screen the charge of PG head groups as efficient as K^+ ions at double concentration and reduce the head group area. Thus, the net outcome of such interaction can be quite complex as it depends on ion type-dependent screening of the DNA charge, ion and lipid head group type–dependent screening of the membrane charge, ion type-dependent compression of the membrane and the conformation of the DNA molecule.

Indeed, we find the affinity of DNA to lipid membrane to also depend on whether DNA is single or double stranded. For example, dsDNA has a higher affinity than ssDNA of the same length on both PE/PC and PE/PG membranes despite carrying double the negative charge (Figure 4A and 4B, respectively; red bars). We attribute this behavior to the differences in the DNA conformation: a mushroom-like conformation of ssDNA brings its negative charges closer, on average, than straight up conformation of dsDNA (see simulation results below, Fig. 5A and 5B). However, this is only the case for 0.3 M KCl whereas in PBS there is no uniform trend (Figure 4A and 4B, yellow bars). Such buffer dependence could be explained by better screening of the electrical charges in the case of the PBS buffer, which would lessen the electrostatic penalty for both molecules. Overall, the data suggest that the dependence of affinity on lipid-head group and buffer type can be rationalized considering electrostatic interactions between DNA and membrane head-groups, and the additional influence of buffer composition on charge screening. But in several cases, the interplay between the factors is more complex and has to consider the conformation and length of the DNA strand.

Visualization of DNA Characteristics on the Nanoscale through MD Simulations.

To elucidate the microscopic bilayer interactions and configurations adopted by DNA molecules tethered to different lipid bilayers, we built six microscopic models of the experimental systems, Figure 5. Each system contained four copies of either dsDNA or ssDNA molecules each conjugated to a cholesterol linker, a patch of a pure POPE (PE) membrane or a patch of 50/50 POPE/POPG (PE/PG) or POPE/POPC (PE/PC) lipid mixture and 300 mM KCl solution, see top panels of Figures 5A, 5B. The six systems were equilibrated for 300 ns each, the final configurations of the DNA molecules are shown at the bottom panels of Figures 5A, 5B. See Methods for detailed description of simulation protocols.

During the MD simulations, the configuration of DNA molecules deviated significantly from their initial idealized conformations (Figure 5A, B, and Figure S3 and Movies 1–6). Significant differences in the conformations of dsDNA and ssDNA molecules can be seen regardless of the lipid bilayer type: while dsDNA molecules maintained largely upright conformations (Figure 5C, Figure S4) ssDNA molecules collapsed, forming a polymer brush. The propensity of DNA molecules to forming contact with lipid bilayer membranes clearly depended not only the type of the DNA molecules (ssDNA versus dsDNA), but also on the lipid bilayer composition (Figure 5D, Figure S5). Thus, more than 20% of all nucleotides of ssDNA formed stable contacts with the head groups of PE or PE/PC bilayers, whereas the presence of PG head groups prevented such contacts from forming. The

differential affinity of DNA molecules to the lipid bilayer containing 50% PG head groups is explained by the negative charge of the PG groups, which repels negatively charged DNA.

The composition of a lipid bilayer is found to have a measurable effect of the manner the DNA-cholesterol conjugates are anchored to the membrane. The repulsive electrostatic interaction between DNA and PG head groups produced stretching of the linker, increasing the distance between the cholesterol moiety and the proximal fragments of DNA in comparison to the configurations observed for pure PE or PE/PC membrane systems (Figure 5E, Figure S6). The effect becomes even more significant when looking at the average distance between the lipid head groups and the proximal fragments of DNA (Figure 5F, Figure S7). Conversely, cholesterol anchors are found to locate closer to the lipid head groups in the case of the PE/PG bilayer (Figure 5G, Figure S8). All of the above suggests that the composition of lipid membranes can have a considerable effect on stability of cholesterol-anchored DNA molecules, and that DNA tethering to PE/PG mixture is considerably less stable than that to pure PE or mixed PE/PC membranes. These conclusions apply to both, dsDNA and ssDNA.

Finally, we note that, while being tethered to lipid bilayers, the DNA molecules are free to diffuse along the membrane surface. Figure 5H plots the diffusion constants of the cholesterol anchors linked to ssDNA and dsDNA molecules in the lipid membranes of the three compositions. The diffusion of the anchors is found to be similar for ssDNA- and dsDNA-conjugated molecules, suggesting that that resistance of the lipid bilayer determines the rate of diffusion of the cholesterol-DNA complexes. At the same time, we find diffusion of cholesterol anchors in the PE/PG membrane to be slower than that in pure PE or PE/PC mixture membranes. We attribute this observation to a shallower placement of the anchors in the PE/PG membrane (Figure 5G). Indeed, rich in hydrogen bonds and salt-bridge interactions, lipid head group environment can be expected to provide more resistance to cholesterol diffusion than the hydrophobic environment of lipid tails.

CONCLUSIONS

Given the versatile use of membrane-tethered DNA in several research areas, this study has examined how cholesterol-modified DNA strands anchor and interacts with lipid bilayers. Biophysical insight is relevant and can guide the future design of membrane-interacting DNA nanostructures such as by tuning the membrane affinity of DNA strands, or by choosing conditions to enhance the molecular accessibility of DNA for hybridization to functional molecular cargo.

As first insight, the K_d values of lipid-anchored DNA to membranes are reported. Previously, this important biophysical data was not known. Second, ionic interaction is a main factor influencing membrane tethering. Electrostatic repulsion between negatively charged DNA and similarly charged lipid head groups strongly reduces affinity of the interaction. Electrostatic screening of negative charges by counter ions can compensate this effect. Microscopic visualization with molecular dynamics concurs and adds further insight to the role or electrostatics. Repulsion leads to a minimal contact between DNA and

membrane, an increased stretching of DNA and linker relative to the membrane-inserted cholesterol, and a faster lateral diffusion of the DNA in the membrane.

In addition to electrostatics, the study underscores the role of sterics. In molecular visualization, the single vs. double-stranded DNA exhibit different dynamic structures on membranes. While dsDNA molecules maintain largely upright conformations, ssDNA molecules collapse to form a polymer brush. The collapse is accompanied by an increased contact to the membrane, provided there are positive charges in the lipid head groups. The conformational differences between single and double stranded DNA are expected to influence the respective molecular accessibility on membrane interfaces.

By synergistically combining experiment and computational simulations, the new insight can be used by researchers in the field of DNA nanotechnology or biophysics to improve the design of DNA strands or choice of lipids to facilitate hybridization at membranes For example, if single-stranded DNA is used, negatively charged as opposed to zwitterionic lipids are suggested to lead to more steric accessibility of the bases for hybridization, although at the cost of lower affinity of membrane anchoring. Furthermore, as double stranded DNA has the weakest backbone interaction to the membranes, another practically relevant suggestion is to attain DNA hybrdiziation with a new strand via toe-hold mediated strand displacement as opposed to simple single strand association. In conclusion, our report delivers fundamental scientific insight of DNA at bilayer interfaces and provides new scope for the development of DNA nanotechnology and synthetic biology.

METHODS

Materials:

Unmodified and cholesterol-labeled DNA oligonucleotides were purchased from Integrated DNA Technologies on a 100 nmol scale with HPLC or PAGE purification. 1,2-dioleoyl-*sn*-glycero-3-phosphoethanolamine (PE), 1,2-dioleoyl-*sn*-glycero-3-phosphocholine (PC) and 1,2-dioleoyl-*sn*-glycero-3-phospho-(1′-rac-glycerol) (PG) were procured from Avanti Polar Lipids. All other reagents and solvents were purchased from Sigma-Aldrich.

DNA duplex formation:

DNA oligonucleotides were dissolved in deionized water at a concentration of 10 μM prior to dilution in the experimental buffers PBS (10 mM PO_4^{3-}, 137 mM NaCl, 2.7 mM KCl, pH = 7.4) or KCl (0.3 M KCl, 15 mM Tris pH 8.0). DNA duplexes were obtained by a preparing an equimolar mixture of DNA strands at a final concentration of 10 μM, and incubating the mix for 2 min at 95 °C followed by cooling to 20 °C at a rate of 5 °C per min using a PCR thermocycler. The sequences of the DNA oligonucleotides are: 20 nt, 5′-TAG TCG ATT TTA TCC ATG CA-TEG-cholesterol-3′; 20 nt compliment 5′-TGC ATG GAT AAA ATC GAC TA-3′. 40 nt, 5′-CAT TTT TCC ACG TTC GCT AAT AGT CGA TTT TAT CCA TGC A-TEG-cholesterol-3′; 40 nt compliment, 5′-TGC ATG GAT AAA ATC GAC TAT TAG CGA ACG TGG AAA AAT G-3′.

Preparation of SUVs:

A solution of lipids PE (0.3 mmol, 50 μl) and PC (0.7 mmol, 550 μl), or PG (0.2 mmol, 100 μl) and PE (0.8 mmol, 59.5 μl) in chloroform was added to a 5 ml round bottom flask. The solvent was removed using a rotary evaporator to yield a thin film, which was subsequently dried under ultrahigh vacuum for 3 h. The lipid was re-suspended in buffer 0.3 M KCl, 15 mM Tris pH 8.0 or PBS (1 ml), and the solution was sonicated for 30 min at RT. SUVs were left to equilibrate for 5 h and used within 24 h. The suspension was gently resuspended 2 s before use. SUVs were subjected to dynamic light scattering (DLS) to confirm the vesicles' diameter using a Zetasizer Nano S from Malvern. The diameters and PDIs were 69 ± 8 nm and 0.23 for PE/PG, and 106 ± 3 nm and 0.76 for PE/PC vesicles, respectively.

DNA-SUV binding assay and agarose gel electrophoresis:

The binding assay was conducted by mixing DNA solutions (10 μM, 10 μl; 20 ss, 20 ds, 40 ss or 40 ds) with a suspension of PC/PE or PG/PE vesicles (1 mM lipid, 0 – 21.6 μl, end concentration of 0 – 250 μM). The DNA SUV mixture was incubated for 20 min at RT. The mix was analyzed using 2 % agarose gel in TAE buffer pH 8.0. To load samples on the gel, the DNA SUV mix (40 μl) was combined with a solution (10 μl) of 60% glycerol. The gel was run at 60 V for 60 min at 20°C. The bands were visualized by ultraviolet illumination after staining with ethidium bromide solution. A 100-base-pair marker (New England Biolabs) was used as the reference standard.

MD Methods:

All atom models of dsDNA and ssDNA molecules were created using the NAB module of AmberTools.[15] An additional nucleotide was added to DNA to covalently conjugate the cholesterol molecule via the TEG linker as described previously.[47] The initial configurations of the lipid bilayer membrane were generated from the CHARMM-GUI membrane builder.[48] Three types of membrane systems were built, each containing a 10 nm × 10 nm patch of either pure POPE (PE) membrane or a 50/50 mixture of POPE/POPG (PE/PG) or POPE/POPC (PE/PC) lipids. Next, the four cholesterol-modified DNA molecules were merged with the lipid membranes by placing cholesterol anchors below the plane of lipid head groups of the nearest leaflet and arranging the DNA molecules, within the membrane plane, on a square 5 nm on side. All lipid molecules located within 3 Å of the DNA atoms were removed. The systems were then solvated with TIP3P water[49] using the Solvate plugin of VMD;[50] potassium and chloride ions were added to produce an electrically neutral solution of 0.3 M salt concentration using and Autoionize plugin of VMD.[50] The final structures contained approximately 150,000 atoms.

The assembled systems were subjected to energy minimization using the conjugate gradient method that removed steric clashes between the solute and solvent atoms. During the minimization, all non-hydrogen atoms of DNA and membrane were harmonically restrained to their initial coordinates (with the spring constants of 1 kcal/mol $Å^{-2}$). Subsequently, each system was equilibrated at constant number of atoms (N), constant pressure (P=1 bar) and constant temperature (T=300 K), i.e., an NPT ensemble without any restraints. The Nose-Hoover Langevin piston[51–52] and Langevin thermostat were used to maintain the constant pressure and temperature in the system.[53] CHARMM36 force field parameters described the

bonded and non-bonded interactions of among DNA, lipid bilayer membranes, water and ions[54] along with NBFIX corrections for non-bonded interaction.[55–57] Parameters for the cholesterol anchor were obtained using the CHARMM general force fields.[58] All atom equilibrium MD simulation were performed using NAMD2 program with periodic boundary conditions and particle mesh Ewald (PME) method to calculate the long range electrostatic interactions.[59] A 8–10-12 Å cutoff scheme was used to calculate van der Waals and short range electrostatics forces. All simulations were performed using 2–2-6 multiple time steps for integrating the equation of motion. SETTLE algorithm[60] was applied to keep water molecules rigid whereas RATTLE algorithm[61] constrained all other covalent bonds involving hydrogen atoms. A 300 ns equilibrium MD simulation was performed for each system, which we found to be sufficient for the four DNA molecules to adopt statistically similar equilibrium conformations. The coordinates of the system were saved at the interval of 9.6 ps simulation. The analysis and post processing the simulation trajectories were performed using VMD[50] and CPPTRAJ.[62]

Supplementary Material

Refer to Web version on PubMed Central for supplementary material.

ACKNOWLEDGMENT

We thank Conor Lanphere for contributing to the literature research and calculating the surface density of DNA, and Christoph Salzmann for discussing the biophysical analysis of membrane binding.

Funding Sources

S.H. and P.A. acknowledge support by and the National Physical Laboratory. S.H. is supported by the EPSRC (EP/N009282/1), the BBSRC (BB/M025373/1, BB/N017331/1), and the Leverhulme Trust (RPG-2017-015). A.A. and H.J. acknowledge the support from the National Science Foundation under Grants DMR-1827346 and DMR-1507985 and National Institutes of Health grant P41-GM104601 and the supercomputer time provided through XSEDE Allocation Grant MCA05S028 and the Blue Waters petascale supercomputer system (UIUC). H.J. acknowledges an Oversee Visiting Fellowship in Nano Science & Technology from Indian Department of Science and Technology.

ABBREVIATIONS

DNA	deoxyribose nucleic acid
HPLC	high pressure liquid chromatography
PAGE	polyacrylamide gel electrophoresis
PC	1,2-dioleoyl-*sn*-glycero-3-phosphocholine
PE	1,2-dioleoyl-*sn*- glycero-3-phosphoethanolamine
PG	1,2-dioleoyl-*sn*-glycero-3-phospho-*rac*-(1′-glycerol)
SUV	small unilamellar vesicle

REFERENCES

(1). Lopez A; Liu J DNA Oligonucleotide-Functionalized Liposomes: Bioconjugate Chemistry, Biointerfaces, and Applications. Langmuir 2018.

(2). Yoshina-Ishii C; Boxer SG Arrays of Mobile Tethered Vesicles on Supported Lipid Bilayers. J. Am. Chem. Soc 2003, 125, 3696–3697. [PubMed: 12656589]

(3). Banchelli M; Gambinossi F; Durand A; Caminati G; Brown T; Berti D; Baglioni P Modulation of Density and Orientation of Amphiphilic DNA on Phospholipid Membranes. Ii. Vesicles. J. Phys. Chem. B 2010, 114, 7348–7358. [PubMed: 20446699]

(4). Gambinossi F; Banchelli M; Durand A; Berti D; Brown T; Caminati G; Baglioni P Modulation of Density and Orientation of Amphiphilic DNA Anchored to Phospholipid Membranes. I. Supported Lipid Bilayers. J. Phys. Chem. B 2010, 114, 7338–7347. [PubMed: 20446700]

(5). Schade M; Berti D; Huster D; Herrmann A; Arbuzova A Lipophilic Nucleic Acids--a Flexible Construction Kit for Organization and Functionalization of Surfaces. Adv. Colloid Interfac 2014, 208, 235–251.

(6). Loew M; Springer R; Scolari S; Altenbrunn F; Seitz O; Liebscher J; Huster D; Herrmann A; Arbuzova A Lipid Domain Specific Recruitment of Lipophilic Nucleic Acids: A Key for Switchable Functionalization of Membranes. J. Am. Chem. Soc 2010, 132, 16066–16072. [PubMed: 20964327]

(7). Jungmann R; Steinhauer C; Scheible M; Kuzyk A; Tinnefeld P; Simmel FC Single-Molecule Kinetics and Super-Resolution Microscopy by Fluorescence Imaging of Transient Binding on DNA Origami. Nano Lett. 2010, 10, 4756–4761. [PubMed: 20957983]

(8). Iinuma R; Ke Y; Jungmann R; Schlichthaerle T; Woehrstein JB; Yin P Polyhedra Self-Assembled from DNA Tripods and Characterized with 3d DNA-Paint. Science 2014, 344, 65–69. [PubMed: 24625926]

(9). Langecker M; Arnaut V; List J; Simmel FC DNA Nanostructures Interacting with Lipid Bilayer Membranes. Acc. Chem. Res 2014, 47, 1807–1815. [PubMed: 24828105]

(10). Zhang Z; Yang Y; Pincet F; M, C. L.; Lin C Placing and Shaping Liposomes with Reconfigurable DNA Nanocages. Nat. Chem 2017, 9, 653–659. [PubMed: 28644472]

(11). Birkholz O; Burns JR; Richter CP; Psathaki OE; Howorka S; Piehler J Multi-Functional DNA Nanostructures That Puncture and Remodel Lipid Membranes into Hybrid Materials. Nat. Commun 2018, 9, 1521. [PubMed: 29670084]

(12). Franquelim HG; Khmelinskaia A; Sobczak JP; Dietz H; Schwille P Membrane Sculpting by Curved DNA Origami Scaffolds. Nat. Commun 2018, 9, 811. [PubMed: 29476101]

(13). Langecker M; Arnaut V; Martin TG; List J; Renner S; Mayer M; Dietz H; Simmel FC Synthetic Lipid Membrane Channels Formed by Designed DNA Nanostructures. Science 2012, 338, 932–936. [PubMed: 23161995]

(14). Howorka S Nanotechnology. Changing of the Guard. Science 2016, 352, 890–891. [PubMed: 27199400]

(15). Burns J; Stulz E; Howorka S Self-Assembled DNA Nanopores That Span Lipid Bilayers. Nano Lett. 2013, 13, 2351–2356. [PubMed: 23611515]

(16). Gopfrich K; Zettl T; Meijering AE; Hernandez-Ainsa S; Kocabey S; Liedl T; Keyser UF DNA-Tile Structures Induce Ionic Currents through Lipid Membranes. Nano Lett. 2015, 15, 3134–3138. [PubMed: 25816075]

(17). Burns JR; Seifert A; Fertig N; Howorka S A Biomimetic DNA-Based Channel for the Ligand-Controlled Transport of Charged Molecular Cargo across a Biological Membrane. Nat. Nanotechnol 2016, 11, 152–156. [PubMed: 26751170]

(18). Maingi V; Burns JR; Uusitalo JJ; Howorka S; Marrink SJ; Sansom MS Stability and Dynamics of Membrane-Spanning DNA Nanopores. Nat. Commun. 2017, 8, 14784. [PubMed: 28317903]

(19). Howorka S; Siwy Z Nanopore Analytics: Sensing of Single Molecules. Chem. Soc. Rev 2009, 38, 2360–2384. [PubMed: 19623355]

(20). Liu L; Wu HC DNA-Based Nanopore Sensing. Angew. Chem. Int. Ed 2016, 55, 15216–15222.

(21). Stoloff DH; Wanunu M Recent Trends in Nanopores for Biotechnology. Curr. Opin. Biotechnol 2013, 24, 699–704. [PubMed: 23266100]

(22). Dutta PK; Zhang Y; Blanchard AT; Ge C; Rushdi M; Weiss K; Zhu C; Ke Y; Salaita K Programmable Multivalent DNA-Origami Tension Probes for Reporting Cellular Traction Forces. Nano Lett 2018.

(23). Ohmann A; Li CY; Maffeo C; Al Nahas K; Baumann KN; Gopfrich K; Yoo J; Keyser UF; Aksimentiev A A Synthetic Enzyme Built from DNA Flips 10(7) Lipids Per Second in Biological Membranes. Nat. Commun 2018, 9, 2426. [PubMed: 29930243]

(24). Chung M; Boxer SG Stability of DNA-Tethered Lipid Membranes with Mobile Tethers. Langmuir 2011, 27, 5492–5497. [PubMed: 21452847]

(25). Ries O; Loffler PM; Vogel S Convenient Synthesis and Application of Versatile Nucleic Acid Lipid Membrane Anchors in the Assembly and Fusion of Liposomes. Org. Biomol. Chem 2015, 13, 9673–9680. [PubMed: 26264076]

(26). Beales PA; Vanderlick TK Specific Binding of Different Vesicle Populations by the Hybridization of Membrane-Anchored DNA. J. Phys. Chem. A 2007, 111, 12372–12380. [PubMed: 17997531]

(27). Peng R; Wang H; Lyu Y; Xu L; Liu H; Kuai H; Liu Q; Tan W Facile Assembly/Disassembly of DNA Nanostructures Anchored on Cell-Mimicking Giant Vesicles. J. Am. Chem. Soc 2017, 139, 12410–12413. [PubMed: 28841373]

(28). Stengel G; Zahn R; Hook F DNA-Induced Programmable Fusion of Phospholipid Vesicles. J. Am. Chem. Soc 2007, 129, 9584–9585. [PubMed: 17629277]

(29). Flavier KM; Boxer SG Vesicle Fusion Mediated by Solanesol-Anchored DNA. Biophys. J 2017, 113, 1260–1268. [PubMed: 28647061]

(30). van Lengerich B; Rawle RJ; Bendix PM; Boxer SG Individual Vesicle Fusion Events Mediated by Lipid-Anchored DNA. Biophys. J 2013, 105, 409–419. [PubMed: 23870262]

(31). Beales PA; Vanderlick TK Application of Nucleic Acid-Lipid Conjugates for the Programmable Organisation of Liposomal Modules. Adv. Colloid Interfac 2014, 207, 290–305.

(32). Beales PA Biophysics: A Toehold in Cell Surface Dynamics. Nat. Nanotechnol 2017, 12, 404–406. [PubMed: 28319614]

(33). Loffler PMG; Ries O; Rabe A; Okholm AH; Thomsen RP; Kjems J; Vogel S A DNA-Programmed Liposome Fusion Cascade. Angew. Chem. Int. Ed 2017, 56, 13228–13231.

(34). Ash WL; Zlomislic MR; Oloo EO; Tieleman DP Computer Simulations of Membrane Proteins. Biochim. Biophys. Acta 2004, 1666, 158–189. [PubMed: 15519314]

(35). Piggot TJ; Pineiro A; Khalid S Molecular Dynamics Simulations of Phosphatidylcholine Membranes: A Comparative Force Field Study. J. Chem. Theory Comput 2012, 8, 4593–4609. [PubMed: 26605617]

(36). Khalili-Araghi F; Gumbart J; Wen PC; Sotomayor M; Tajkhorshid E; Schulten K Molecular Dynamics Simulations of Membrane Channels and Transporters. Curr. Opin. Struct. Biol 2009, 19, 128–137. [PubMed: 19345092]

(37). Petrache HI; Dodd SW; Brown MF Area Per Lipid and Acyl Length Distributions in Fluid Phosphatidylcholines Determined by (2)H Nmr Spectroscopy. Biophys. J 2000, 79, 3172–3192. [PubMed: 11106622]

(38). Fogarty JC; Arjunwadkar M; Pandit SA; Pan J Atomically Detailed Lipid Bilayer Models for the Interpretation of Small Angle Neutron and X-Ray Scattering Data. Biochim. Biophys. Acta 2015, 1848, 662–672. [PubMed: 25448879]

(39). Chiu SW; Pandit SA; Scott HL; Jakobsson E An Improved United Atom Force Field for Simulation of Mixed Lipid Bilayers. J. Phys. Chem. B 2009, 113, 2748–2763. [PubMed: 19708111]

(40). Harper PE; Mannock DA; Lewis RN; McElhaney RN; Gruner SM X-Ray Diffraction Structures of Some Phosphatidylethanolamine Lamellar and Inverted Hexagonal Phases. Biophys. J 2001, 81, 2693–2706. [PubMed: 11606282]

(41). Banchelli M; Gambinossi F; Durand A; Caminati G; Brown T; Berti D; Baglioni P Modulation of Density and Orientation of Amphiphilic DNA on Phospholipid Membranes. Ii. Vesicles. J. Phys. Chem. B 2010, 114, 7348–7358. [PubMed: 20446699]

(42). Bai Y; Greenfeld M; Travers KJ; Chu VB; Lipfert J; Doniach S; Herschlag D Quantitative and Comprehensive Decomposition of the Ion Atmosphere around Nucleic Acids. J. Am. Chem. Soc 2007, 129, 14981–14988. [PubMed: 17990882]

(43). Yoo J; Aksimentiev A Competitive Binding of Cations to Duplex DNA Revealed through Molecular Dynamics Simulations. J. Phys. Chem. B 2012, 116, 12946–12954. [PubMed: 23016894]

(44). Cheng Y; Korolev N; Nordenskiold L Similarities and Differences in Interaction of K+ and Na+ with Condensed Ordered DNA. A Molecular Dynamics Computer Simulation Study. Nucleic Acids Res. 2006, 34, 686–696. [PubMed: 16449204]

(45). Gurtovenko AA; Vattulainen I Effect of Nacl and Kcl on Phosphatidylcholine and Phosphatidylethanolamine Lipid Membranes: Insight from Atomic-Scale Simulations for Understanding Salt-Induced Effects in the Plasma Membrane. J. Phys. Chem. B 2008, 112, 1953–1962. [PubMed: 18225878]

(46). Joshi H; Maiti PK Structure and Electrical Properties of DNA Nanotubes Embedded in Lipid Bilayer Membranes. Nucleic Acids Res. 2018, 46, 2234–2242. [PubMed: 29136243]

(47). Gopfrich K; Li CY; Ricci M; Bhamidimarri SP; Yoo J; Gyenes B; Ohmann A; Winterhalter M; Aksimentiev A; Keyser UF Large-Conductance Transmembrane Porin Made from DNA Origami. ACS Nano 2016, 10, 8207–8214. [PubMed: 27504755]

(48). Jo S; Kim T; Iyer VG; Im W Charmm-Gui: A Web-Based Graphical User Interface for Charmm. J. Comput. Chem 2008, 29, 1859–1865. [PubMed: 18351591]

(49). Jorgensen WL; Chandrasekhar J; Madura JD; Impey RW; Klein ML Comparison of Simple Potential Functions for Simulating Liquid Water. J. Chem. Phys 1983, 79, 926–935.

(50). Humphrey W; Dalke A; Schulten K Vmd: Visual Molecular Dynamics. J. Mol. Graph. Model 1996, 14, 33–38.

(51). Feller SE; Zhang YH; Pastor RW; Brooks BR Constant-Pressure Molecular-Dynamics Simulation - the Langevin Piston Method. J. Chem. Phys 1995, 103, 4613–4621.

(52). Martyna GJ; Tobias DJ; Klein ML Constant-Pressure Molecular-Dynamics Algorithms. J. Chem. Phys 1994, 101, 4177–4189.

(53). Sindhikara DJ; Kim S; Voter AF; Roitberg AE Bad Seeds Sprout Perilous Dynamics: Stochastic Thermostat Induced Trajectory Synchronization in Biomolecules. J. Chem. Theory Comput 2009, 5, 1624–1631. [PubMed: 26609854]

(54). Hart K; Foloppe N; Baker CM; Denning EJ; Nilsson L; MacKerell AD Optimization of the Charmm Additive Force Field for DNA: Improved Treatment of the Bi/Bii Conformational Equilibrium. J. Chem. Theory Comput 2012, 8, 348–362. [PubMed: 22368531]

(55). Yoo J; Aksimentiev A New Tricks for Old Dogs: Improving the Accuracy of Biomolecular Force Fields by Pair-Specific Corrections to Non-Bonded Interactions. Phys. Chem. Chem. Phys 2018, 20, 8432–8449. [PubMed: 29547221]

(56). Yoo J; Aksimentiev A Improved Parameterization of Amine-Carboxylate and Amine-Phosphate Interactions for Molecular Dynamics Simulations Using the Charmm and Amber Force Fields. J. Chem. Theory Comput 2016, 12, 430–443. [PubMed: 26632962]

(57). Yoo JJ; Aksimentiev A Improved Parametrization of Li+, Na+, K+, and Mg2+ Ions for All-Atom Molecular Dynamics Simulations of Nucleic Acid Systems. J. Phys. Chem. Lett 2012, 3, 45–50.

(58). Vanommeslaeghe K; MacKerell AD Automation of the Charmm General Force Field (Cgenff) I: Bond Perception and Atom Typing. J. Chem. Inf. Model 2012, 52, 3144–3154. [PubMed: 23146088]

(59). Phillips JC; Braun R; Wang W; Gumbart J; Tajkhorshid E; Villa E; Chipot C; Skeel RD; Kale L; Schulten K Scalable Molecular Dynamics with Namd. J. Comput. Chem 2005, 26, 1781–1802. [PubMed: 16222654]

(60). Miyamoto S; Kollman PA Settle - an Analytical Version of the Shake and Rattle Algorithm for Rigid Water Models. J. Comput. Chem 1992, 13, 952–962.

(61). Andersen HC Rattle - a Velocity Version of the Shake Algorithm for Molecular-Dynamics Calculations. J. Comput. Phys 1983, 52, 24–34.

(62). Roe DR; Cheatham TE Ptraj and Cpptraj: Software for Processing and Analysis of Molecular Dynamics Trajectory Data. J. Chem. Theory Comput 2013, 9, 3084–3095. [PubMed: 26583988]

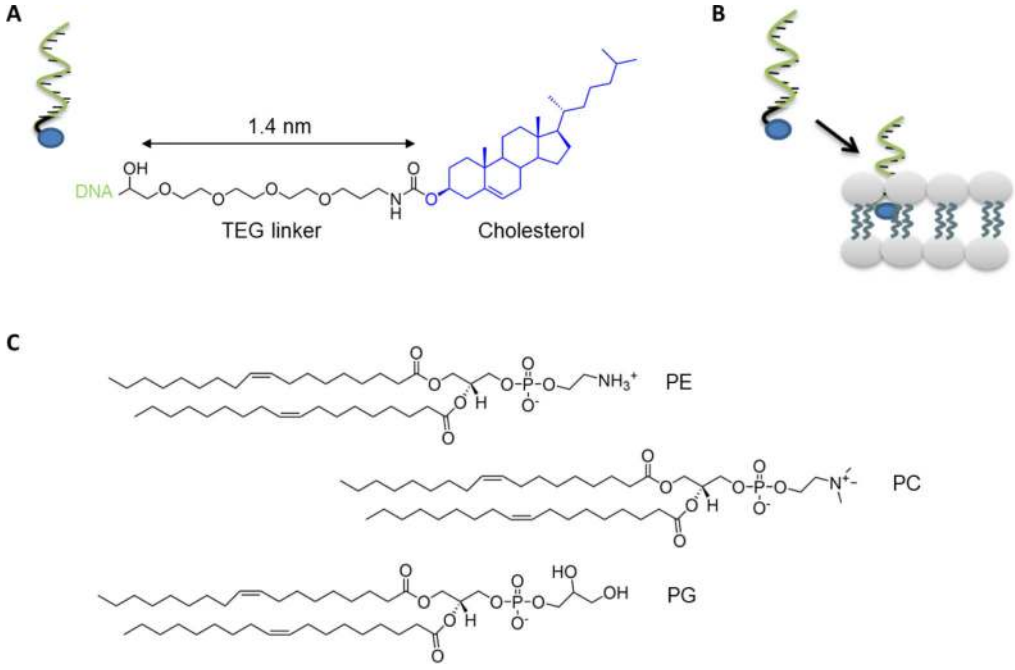

Figure 1:

Molecular components used to probe the interaction between lipid-modified DNA and bilayer membranes. (A) DNA oligonucleotide carrying a 5′-terminal cholesterol via a TEG linker. (B) Schematic drawing on a cholesterol-modified DNA oligonucleotide inserted into a lipid bilayer. (C) Phospholipids 1,2-dioleoyl-*sn*-glycero-3-phosphoethanolamine (PE), 1,2-dioleoyl-*sn*-glycero-3-phosphocholine (PC), and 1,2-dioleoyl-*sn*-glycero-3-phospho-*rac*-(1′-glycerol) (PG).

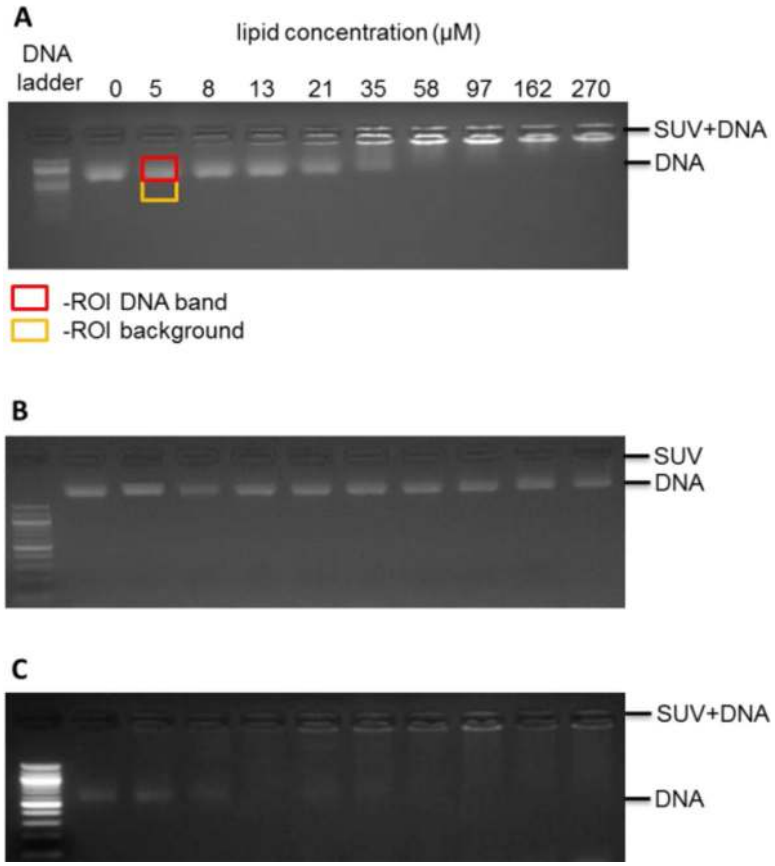

Figure 2:

Gel shift assay to determine the extent of membrane binding for cholesterol-modified DNA strands. The assay discriminates free DNA that migrates into the agarose gel and membrane vesicle-bound DNA at the gel top. Increasing the concentration of lipid membrane vesicles (0–250 μM lipid) changes the proportion of DNA from free to the bound state. (A) Titration result for the binding of cholesterol-modified 20 nt ssDNA to PE/PC vesicles in PBS. The red box around the free DNA band was used to determine the band intensity which was corrected for the background of the gel (orange box). See text for more details. (B) The titration read-out for 20-nt ssDNA against PE/PG in 0.3 M KCl reveals a weak extent of membrane binding. (C) A strong interaction is found for 20 nt dsDNA to PE/PG in 0.3 M KCl.

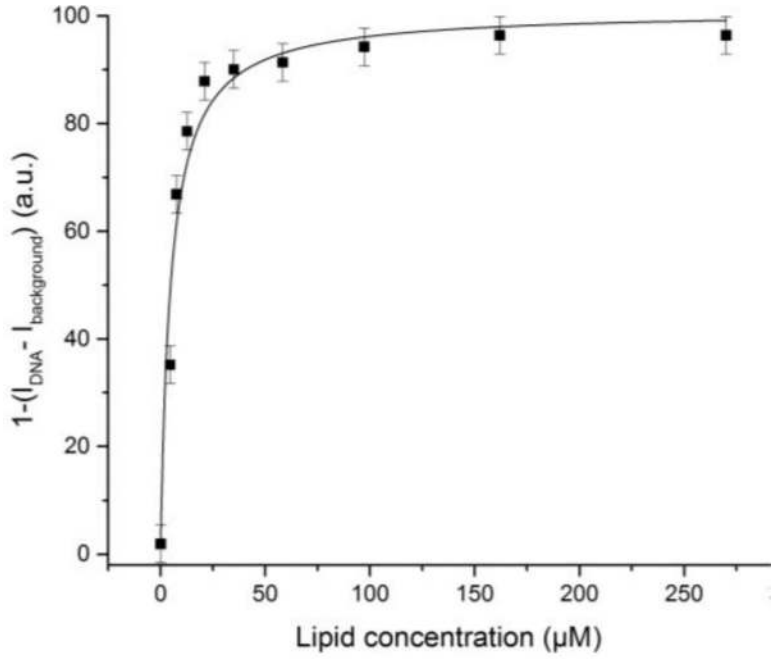

Figure 3:

Quantitative analysis of the gel-shift data with a plot of gel intensity-derived value of 1-(I_{DNA} - $I_{background}$) which is equivalent to the normalized amount of SUV-bound DNA, vs the concentration of lipid used to generate SUVs. The analysis is for the binding of cholesterol-modified dsDNA of 20 nt to PE/PC vesicles in 0.3 M KCl. The averages and standard deviations represent data from 3 independent experiments.

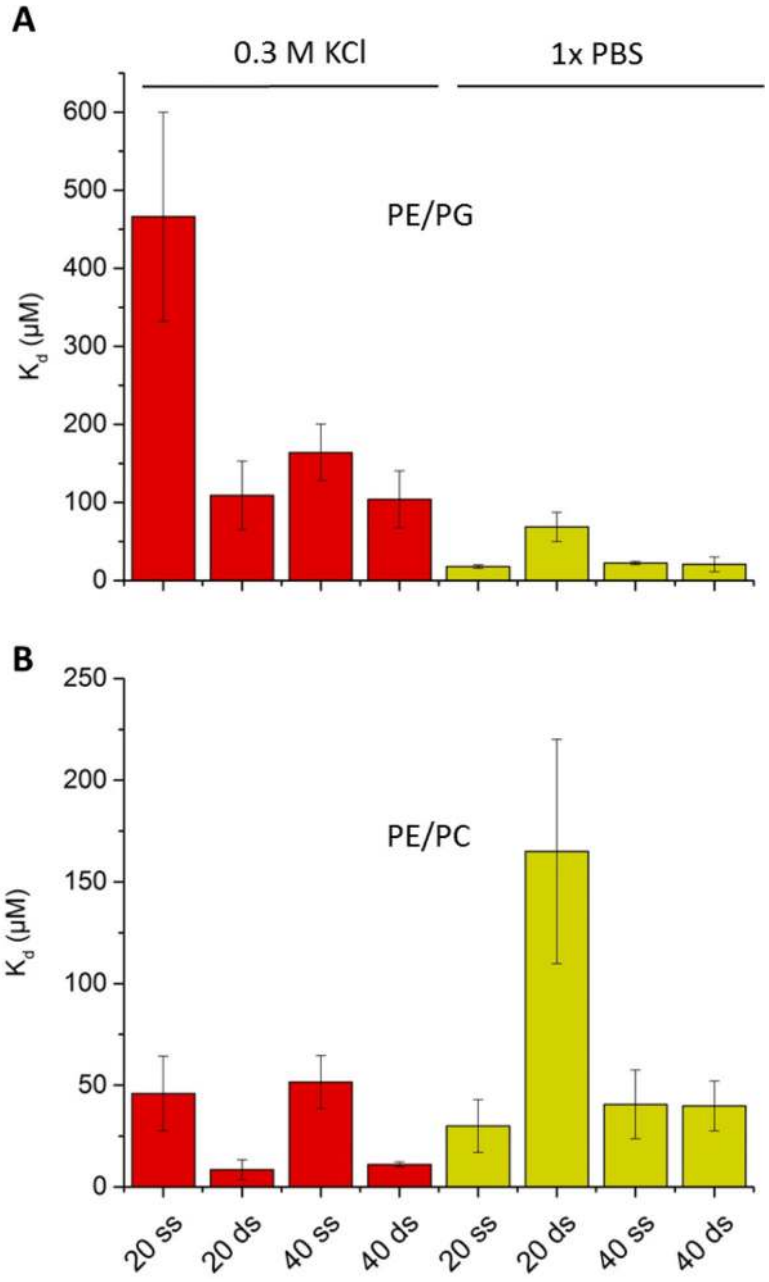

Figure 4:

K_d values obtained from the gel shift assay for DNA strands on PE/PC (A) and PE/PG SUVs (B) in buffers 0.3 M KCl (red columns) or PBS (yellow columns).

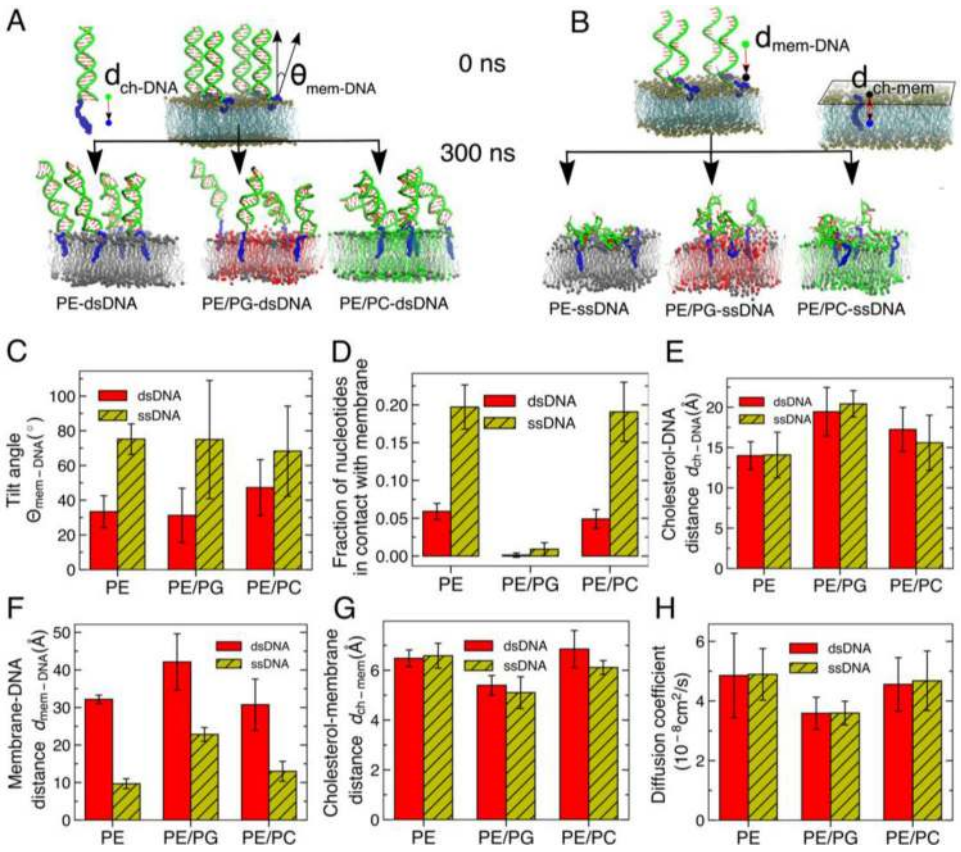

Figure 5:

Molecular dynamics simulations of DNA tethered to lipid bilayer membranes. (A, B) Initial (top) and final (bottom) configurations of the simulation systems. Each system contains four DNA molecules of 20 basepairs (panel A) or nucleotides (panel B). Each molecule is tethered to the lipid bilayers through a cholesterol linker containing an additional nucleotide. The systems are submerged in 0.3 M KCl solution (not shown). (C) Average tilt of the DNA molecules with respect to the bilayer normal, $\theta_{\text{mem-DNA}}$. (D) Fraction of DNA nucleotides in contacts with the lipid bilayer within the last 30 ns of the respective equilibration trajectory. A contact was defined as a having a C3' atom of DNA backbone located within 5 Å of any non-hydrogen atoms of the membrane. (E) Average distance between cholesterol and the nearest dsDNA basepair or the second nearest ssDNA nucleotide, $d_{\text{ch-DNA}}$. (F) Average distance between the DNA molecules and the nearest (upper) leaflet of the membrane, $d_{\text{mem-DNA}}$. (G) Average distance between cholesterol and the phosphate group of the membrane's upper leaflet, $d_{\text{ch-mem}}$. All distances reported in panels E—G were computed using center-of-mass coordinates of the respective groups projected along the bilayer normal and averaged over the last 200 ns of the equilibration trajectories. (H) Diffusion coefficient of cholesterol anchors in different membrane systems. SI Figures S4-S9 illustrate how the above quantities change with simulation time. The error bars show the standard deviation in the averaged values among the four DNA molecules in each simulation system.